

Dissipation of the sectored heliospheric magnetic field near the heliopause: a mechanism for the generation of anomalous cosmic rays

J. F. Drake¹, M. Opher², M. Swisdak¹ and J. N. Chamoun¹

ABSTRACT

The recent observations of the anomalous cosmic ray (ACR) energy spectrum as Voyagers 1 and 2 crossed the heliospheric termination shock have called into question the conventional shock source of these energetic particles. We suggest that the sectored heliospheric magnetic field, which results from the flapping of the heliospheric current sheet, piles up as it approaches the heliopause, narrowing the current sheets that separate the sectors and triggering the onset of collisionless magnetic reconnection. Particle-in-cell simulations reveal that most of the magnetic energy is released and most of this energy goes into energetic ions with significant but smaller amounts of energy going into electrons. The energy gain of the most energetic ions results from their reflection from the ends of contracting magnetic islands, a first order Fermi process. The energy gain of the ions in contracting islands increases their parallel (to the magnetic field \mathbf{B}) pressure p_{\parallel} until the marginal firehose condition is reached, causing magnetic reconnection and associated particle acceleration to shut down. Thus, the feedback of the self-consistent development of the energetic ion pressure on reconnection is a crucial element of any reconnection-based, particle-acceleration model. The model calls into question the strong scattering assumption used to derive the Parker transport equation and therefore the absence of first order Fermi acceleration in incompressible flows. A simple 1-D model for particle energy gain and loss is presented in which the feedback of the energetic particles on the reconnection drive is included. The ACR differential energy spectrum takes the form of a power law with a spectral index slightly above 1.5. The model has the potential to explain several key Voyager observations, including the similarities in the spectra of different ion species.

Subject headings:

¹University of Maryland, College Park, MD 20742; drake@umd.edu, swisdak@umd.edu

²George Mason University, 4400 University Drive, Fairfax, VA 22030; mopher@gmu.edu

1. INTRODUCTION

Anomalous Cosmic Rays (ACRs) are ions that have energies in the range of 5 – 100MeV/nucleon, just below energies associated with galactic cosmic rays. It is known that the ACRs are produced from interstellar neutral atoms since their composition matches that of the local interstellar medium (LISM) (Cummings & Stone 1996, 2007). In the standard model the LISM neutrals are ionized and picked up by the solar wind deep within the heliosphere and carried out to the heliospheric termination shock, where they undergo diffusive shock acceleration (Pesses et al. 1981). The termination shock (TS) marks the transition of the solar wind from supersonic to subsonic flow.

A major surprise when the Voyager spacecraft crossed the TS was that the number density of the ACRs did not peak at the shock (Stone et al. 2005, 2008), indicating that their source was elsewhere. Since Voyager 1’s crossing of the TS in December 2004 and Voyager 2’s crossing in August-September 2007, the two spacecraft have seen increasing intensities of ACRs as they penetrate further into the heliosheath (HS), the subsonic plasma downstream from the shock. One possible explanation for the Voyager observations is that the ACRs peak along the flanks of the heliosphere where the spiral magnetic field from the sun has been in contact with the TS for a longer period of time (McComas & Schwadron 2006). A compressional model of ACRs has also been proposed (Fisk et al. 2006).

Here we suggest that it is not the TS that is the source of the ACRs. Instead it is the annihilation of the “sectored” magnetic field within the heliosheath as it is compressed on its approach to the heliopause (HP) that produces the ACRs. The dipole magnetic field emanating from the sun is quickly dragged in the azimuthal direction due to the sun’s rotation. The resulting azimuthal field B_ϕ reverses sign across the equator with the two polarities separated by the heliospheric current sheet. The difference between the rotation axis of the sun and the magnetic pole of the sun causes the heliospheric current sheet to flap in the vertical direction with a period of 26 days. The resulting folded heliospheric current sheet creates a heliospheric field that displays a “sector” structure consisting of alternating signs of B_ϕ (Wilcox & Ness 1965). The “sector-zone” occupies a latitudinal extent that varies during the solar cycle, reaching nearly the poles when the fields from the sun are a maximum (Smith 2001). The sectors remain a prominent feature of the heliospheric magnetic field out to the TS although the period of the reversals varies erratically from the nominal 13 day value (Burlaga et al. 2003, 2005, 2008). Within the heliosheath the period of the reversals is even more variable, probably a consequence of the low flow speeds in this region and the time-varying location of the TS (Burlaga et al. 2008).

An obvious question is: Why does the sectored azimuthal field survive out to distances of order 90AU? Why don’t the reversed fields simply annihilate as a result of magnetic recon-

nection, releasing the stored magnetic energy? The heliosphere is, for all practical purposes, collisionless. It is well known that the rate of collisionless reconnection drops dramatically when the width of the current channel is greater than the ion inertial scale $d_i = c/\omega_{pi}$ where ω_{pi} is the ion plasma frequency (Yamada 2007; Cassak et al. 2005). At 1AU the current sheet is on average around 10,000km wide, which is in the range of $200d_i$ (Winterhalter et al. 1994; Smith 2001). The deviations from this mean width are substantial and magnetic reconnection is occasionally observed during crossings of the heliospheric current sheet (Gosling et al. 2007). In any case, upstream of the TS the heliospheric current sheet is too wide to expect collisionless reconnection to dissipate the sector zone.

In the present paper we present MHD simulations of the global heliosphere showing the development of the sectorized heliospheric field. The current sheet compresses and the spacing of the current sheets shrinks across the TS. As the plasma in the heliosheath approaches the heliopause its radial motion slows, causing the current sheet widths and sector spacing to further decrease. Current sheets upstream of the Earth’s bow shock have been observed to compress by more than a factor of 30 as they first compress across the shock and then pile up against the magnetopause (Phan et al. 2007). At the same time the magnetic field strength rises and the plasma density and pressure decrease as the plasma is squeezed away from the nose of the heliosphere along the magnetic field. The resulting drop in the local plasma β , the ratio of plasma to magnetic pressure, is similar to that seen just upstream of the Earth’s magnetopause (Crooker 1979).

When the width of the heliospheric current layers separating the sectorized fields approach the ion inertial scale, the sectorized field undergoes magnetic reconnection. In particle-in-cell (PIC) simulations of the sectorized geometry, we demonstrate that essentially all of the magnetic energy in the “sector zone” is released into energetic particles as the sectors form a complex network of interacting magnetic islands.

A number of mechanisms have been proposed to explain ion acceleration during reconnection, mostly to address flare observations (Miller et al. 1997). Parallel electric fields are more important for electrons than ions (Litvinenko 1996; Pritchett 2008) and the localization of parallel electric fields in any case limits their overall importance (Drake et al. 2006; Egedal et al. 2009). The resonance absorption of cascading MHD turbulence resulting from reconnection has also been proposed as an accelerator of ions (Miller 1998) although the mechanism for the efficient generation of this turbulence remains unspecified. The Petschek slow shocks bounding the reconnection outflow have also been proposed as sites of ion acceleration (Tsuneta 1996). However, satellite crossings of these boundary layers indicate that ions are heated upon crossing into the reconnection outflows but do not reveal a significant energetic particle component (Gosling et al. 2005).

We find that the most energetic ions are accelerated through reflection in contracting islands, a first-order Fermi process that was studied earlier for electron acceleration (Drake et al. 2006). The rate of particle energy gain is given by

$$\frac{dE}{dt} = \alpha \left\langle \frac{c_A}{L} \right\rangle E, \quad (1)$$

where $\langle c_A/L \rangle$ is a measure of the rate of contraction of magnetic islands and α is a constant. Importantly, the rate of energy gain is proportional to the particle energy and is independent of the particle mass. The pickup particles gain the most energy and form the ACR spectrum because of their high seed energy. Equation (1) implies that the ACR spectra of ions with different masses are similar because their seed energy and rate of energy gain are identical when expressed on a per nucleon basis. The energy spectra of all species assume a power law with an index of $(3 + \beta_0)/2$, where β_0 is the initial pickup ion β where reconnection onsets. An ACR acceleration model based on the MHD description of turbulent reconnection of the sectored fields has also been recently proposed (Lazarian & Opher 2009) and its relationship with the present work is discussed in Sec. 5.

2. MHD simulations of the sector structure of the heliospheric current sheet

To gain a better understanding of the profiles of the plasma parameters and the sector structure of the magnetic field in the crucial region between the TS and the HP, we have carried out MHD simulations including the tilt in the solar magnetic field with respect to the rotation axis.

Our 3D MHD model includes the major components of the interaction of the solar wind with the interstellar medium: the interplanetary and interstellar magnetic field and the ionized and neutral H atoms that interact through charge exchange. Although the neutral H atoms have a mean free path on the order of $100AU$ and should be treated kinetically, a multi-fluid description (four fluids describing each zone of the interaction) does a comparable job (see *e.g.* (Alexashov & Izmodenov 2005)). There are a total of five hydrogen fluids, one ionized and four neutral populations (Opher et al. 2009) in the model, which is similar to earlier models (Alexashov & Izmodenov 2005; Zank et al. 1996) and was benchmarked with a kinetic model (Izmodenov 2009). The four populations of neutral H atoms are evolved throughout the simulation domain. They represent the particles of interstellar origin, those peaked in the regions between the bow shock and heliopause, the supersonic solar wind, and the compressed region between the termination shock and the heliopause. All four populations are described by separate systems of the Euler equations with corresponding source terms (McNutt et al. 1999). The ionized component interacts with the H neutrals via

charge exchange (Izmodenov 2009).

The parameters for the inner boundary (at $30AU$) are those used by (Izmodenov 2009) to match the observations: a proton density of $8.7 \times 10^{-3} cm^{-3}$, a temperature of $1.087 \times 10^5 K$ and a Parker spiral field of $2nT$ at the equator. The parameters for the density, velocity and temperature for the ions and neutrals at the outer boundary in the interstellar medium reflect the best observational values: a proton density of $0.06 cm^{-3}$, a velocity of $26.3 km/s$, a temperature of $6519K$, a density of neutral H in the LISM of $0.18 cm^{-3}$ with the same velocity and temperature as the LISM protons. The only parameter with significant uncertainty at the outer boundary is the interstellar magnetic field. Both the intensity and the directions have large uncertainties (Opher et al. 2009). We assume an interstellar magnetic field of $4.4 \mu G$ with tilt angles $\beta = 60^\circ$ (the angle between the interstellar magnetic field BISM and the heliospheric equatorial plane) and $\alpha = 20^\circ$ (the angle between BISM and the interstellar wind). These values reproduce the positions of the crossings of the TS by Voyagers 1 and 2 (Stone et al. 2005, 2008).

We tilted the Parker spiral at the inner boundary by 7° with respect to the rotation axis of the sun. A refined grid was designed to resolve the reversals of the heliospheric current sheet. The grid has an inner boundary of $30AU$ and an outer boundary ranging from $-300AU$ to $300AU$ in x, y, and z directions. The computational cell size ranges from $0.07AU$ to $18.75AU$. We used fixed inner boundary conditions for the ionized fluid and soft boundaries for the neutral fluids. The outer boundaries were all outflows with the exception of the -x boundary, where inflow conditions were imposed for the ionized plasma and the neutrals coming from the LISM. In order to bring the TS closer to the inner boundary to better resolve the sector structure in the HS, we artificially lowered the solar wind speed to $300 km/s$.

In Fig. 1(a) we show the total magnetic field B in the $x - z$ plane (color) with the flow stream lines in black. Because of the low solar wind speed the TS moves inward to $50AU$. The oscillating region of low B marks the location of the heliospheric current sheet. Above (below) the current sheet the azimuthal field B_ϕ is positive (negative). The region of sectored magnetic field falls within the oscillations of the current sheet. We emphasize that in spite of the high resolution used in this simulation, the calculation significantly underestimates the oscillation amplitude of the current sheet, which on the basis of observations is expected to occupy a region equatorward of a fixed latitudinal angle that depends modestly on the phase of the solar cycle. At the crossing of the TS by Voyagers 1 and 2 the latitudinal extent of the sector region was 30 degrees and at solar maximum the current sheet can approach the poles. The sector structure is compressed downstream of the TS (the sector spacing decreases from $4.7AU$ to $1.9AU$) and the spacing of the sectors continuously decreases further into the HS

as the radial plasma velocity decreases.

We have also carried out a simulation with no relative tilt of the rotation axes of the sun and magnetic field. This allowed reduced resolution and a much larger simulation domain so that the solar wind velocity could be increased to 417km/s to match the observed values. In this simulation we used the same interstellar magnetic field strength and orientation as in the simulation shown in Fig. 1(a) For this case the heliosphere expands to a size that closely matches the Voyager observations of the location of the TS. In Fig. 1(b) the variation of the plasma density ρ , the magnetic field B and the local plasma β are shown along the stagnation line, similar to that which can be seen near the bottom edge of Fig. 1(a) (see also (Opher et al. 2009)). As the radial velocity decreases as the plasma approaches the stagnation point at the HP, the magnetic field compresses and the plasma squeezes out along the magnetic field causing the density and pressure to drop. These trends cause β to fall below unity.

We emphasize that although the sectorized field region in the simulation in Fig. 1(a) does not overlap the stagnation line (because of the 7° tilt of the magnetic field in the simulation), the Voyager 1 and 2 satellites bracketed the stagnation line at the time of the TS crossing (the tilt at the time was around 30°) and both measure the sectorized magnetic field (Burlaga et al. 2003). Thus, the sectorized magnetic field becomes increasingly compressed on its approach to the HP and locally dominates the pressure, in sharp contrast with the upstream HS.

Magnetic reconnection is expected to sharply onset in the region close to the HP due to the compression of the heliospheric current sheet in this region. In this low β region the available magnetic free energy is sufficient to accelerate the pickup ions to the $10 - 100\text{MeV/nuc}$ range of energies that make up the ACRs. Since this is a crucial result for the energetics of the model to work out, we have checked that the result is not sensitive to the specific boundary conditions used in the simulations shown in Fig. 1. A similar plot of the parameters along the stagnation of line from the simulation of Fig. 1(a) revealed that, while the spatial separation between the TS and HP was smaller, the increase in magnetic field strength and the minimum value of β were essentially identical. Thus, neither the magnitude of the tilt between the magnetic and solar rotation axes nor the solar wind speed alter these crucial results of the MHD simulations. Finally, since the orientation of the interstellar magnetic field also remains uncertain, we carried out simulations to check the sensitivity of the compression of the magnetic field and drop in β to these parameters. The results were essentially identical to those shown in Fig. 1(b).

3. PIC simulations of reconnection and particle acceleration

The MHD model does not reliably describe magnetic reconnection or particle acceleration. We explore both by carrying out 2-D particle-in-cell (PIC) simulations of the sector structure in the heliospheric $x - y$ plane. The simulations are performed with the PIC code p3d (Zeiler et al. 2002) using a periodic equilibrium magnetic field $B_y(x)$ resulting from a series of Harris current sheets of peak density n_0 superimposed on a uniform background of density $n_b = 0.2n_0$. The results are presented in normalized units: the magnetic field to the asymptotic value of the reversed field B_{0y} , the density to n_0 , velocities to the proton Alfvén speed $c_A = B_{0y}/\sqrt{4\pi m_p n_0}$, times to the inverse proton cyclotron frequency in B_{0y} , $\Omega_p^{-1} = m_p c/eB_{0y}$, lengths to the proton inertial length $d_p = c_A/\Omega_p$ and temperatures to $m_p c_A^2$. We define some important scale lengths as follows: $w_0 = 0.5d_p$ is the half-width of an individual current sheet; $L_p = 25.6d_p$ is the separation of neighboring current sheets; $\Delta_x = \Delta_y = 0.05d_p$ are the grid scales; and $L_x = 204.8d_p$ and $L_y = 409.6d_p$ are the lengths of the overall computational domain. Since we are focusing on the ion dynamics, which requires as large a simulation domain as possible, we minimize the separation of scales by using a modest ion to electron mass ratio of 25 and velocity of light c of $15c_A$. The particle temperatures are initially uniform with $T_p = (5/12)m_p c_A^2$ and $T_e = (1/12)m_p c_A^2$. A second set of simulations have been carried out with a small number (5%) of ions with high temperature ($T_p = 12.5m_p c_A^2$) to represent the seed population of ACRs. The average number of particles per cell is 100 outside of the current sheets and the total number of protons plus electrons exceeds eight billion. Reconnection begins from particle noise.

The overall scale sizes of our simulations are much smaller than those of the heliospheric sectorized field. The widths of the sectors upstream of the TS are around $1.7 \times 10^8 km$, which at a density of $0.001/cm^3$, is around $2 \times 10^4 c/\omega_{pi}$. A factor of 40 compression through the shock and the approach to the heliopause brings the spacing down to $4 \times 10^6 km$, or with a density of $0.003/cm^3$, around $1000c/\omega_{pi}$. This sector spacing is clearly much larger than the value of $25.6c/\omega_{pi}$ in our simulations. The value of $25.6c/\omega_{pi}$ was chosen as the minimum value necessary to fully magnetize the ions in the simulations (Mandt et al. 1994), which is a necessary requirement to correctly assess the mechanism for ion acceleration. The simulations reveal, as expected, that islands on adjacent current layers eventually overlap. At this time the rate of magnetic energy dissipation is a maximum and the characteristic width of islands is comparable to the sector spacing. The $25.6c/\omega_{pi}$ size islands are large enough to magnetize ions. We also emphasize that the artificial sector spacing used in the simulations does not affect the ultimate fate of the sectors, that the islands grow to a large enough size to destroy the sector structure. As long as the physical system in the direction along the current layers (the azimuthal direction in the heliosphere) is much longer than the sector spacing, once reconnection onsets the sectors will completely break up into a bath of

merging islands. In our simulations the ratio $L_y/L_p = 16$ is more than sufficient to guarantee that the sectors fully reconnect.

The 2-D assumption is also a limitation of the present model. However, 3-D models of anti-parallel reconnection reveal that the electron current perpendicular to the plane of reconnection causes the x-lines to lengthen so that at late time reconnection becomes quasi two-dimensional (Hesse et al. 2001; Huba & Rudakov 2002; Shay et al. 2003). In contrast, in the presence of a guide field such as in the corona, 3-D magnetic reconnection differs greatly from that in 2-D because magnetic islands with differing pitch can grow in 3-D but not in 2-D (Onofri et al. 2006; Drake et al. 2006).

Reconnection of the current sheet is very sensitive to the initial current layer width w_0 . The growth of islands when $w_0 \gg c/\omega_{pi}$ is strongly inhibited, a result that is consistent with the survival of the sectorized field during its propagation to the outer heliosphere. The observed width of the heliospheric current sheet exhibits large variations (Smith 2001). Within the heliosheath crossing times of the current sheet ranging from a day to 50s, the time resolution of the Voyager magnetometer, have been documented (Burlaga et al. 2008). Deducing the physical width of the current sheet from these crossing times is difficult because of the uncertainty of the relative velocity of the spacecraft and the ambient plasma. For the $100km/s$ flows expected just downstream of the TS, the 50s crossing translates to around $1c/\omega_{pi}$. Further compression of the current layers on their approach to the HP similar to that measured at the magnetopause (Phan et al. 2007) would further reduce w_0 . Thus, the value of $w_0 = 0.5c/\omega_{pi}$ taken in our simulations is reasonable. In any case since there is no obvious process to halt the compression of the current sheets as they approach the heliopause, it seems inevitable that the current layers will compress until reconnection onsets.

In Fig. 2 we show the distribution of the out-of-plane electron current J_{ez} at three times. This simulation includes the ACR seed particles. In (a) at $\Omega_p t = 76$ the islands are growing on each of the current layers. At this point in time, because of their relatively short wavelengths, the islands on each current layer grow independently of those on adjacent current layers. This is evident from the lack of phase correlation between islands and x-lines on adjacent current layers in (a). In the double-tearing mode (Pritchett et al. 1980) magnetic islands on adjacent current layers line up so that an island on one current layer drives the x-line on the adjacent layer. Also in (a) some of these islands are becoming larger by coalescing with their neighbors. The merging process releases substantial energy, essentially all of the energy in the smaller of the merging pairs (Fermo et al. 2009). In (b) at $\Omega_p t = 136$ the islands on adjacent current layers have overlapped and islands between the same and adjacent layers are now merging. Finally in (c) at $\Omega_p t = 176$ merging continues and there is essentially no evidence of the original sectorized magnetic field. At the end of the

simulation at $\Omega_p t = 200$, 72% of the magnetic energy has been released, 71% going into ions and 29% into electrons. The implication of these results is that the sectorized magnetic field will essentially be entirely dissipated as it approaches the HP.

In Fig. 3(a),(b) we show the energy spectra of ions and electrons at times $\Omega_p t = 0, 50, 100$ and 200 . This data is from a simulation without seed ACRs so the acceleration of the core ions can be more clearly seen. High energy tails form on both the electron and ion energy distributions. Most of the energy gain occurs between $50\Omega_p^{-1}$ and $100\Omega_p^{-1}$ when islands between adjacent current layers are reconnecting. Note, however, that the distributions are not of the form of a power law. On the other hand, power laws are not expected since they typically arise when processes leading to energy gain of particles are balanced by loss (Blandford & Eichler 1987; Drake et al. 2006). We note that the energy spectra of Fig. 3 are not sensitive to the sector spacing. The electron and ion energy spectra from simulations with a sector spacing half of that of Fig. 3 are nearly identical.

To gain a better understanding of the mechanism for particle acceleration, and in particular that of the ions, we show in Fig. 4 the spatial distribution of the ion temperature parallel (in (a)) and perpendicular (in (b)) to the local magnetic field at $\Omega_p t = 136$ from the simulation of Fig. 2. Note that the color tables of the two plots are identical so the relative values of T_{\parallel} and T_{\perp} can be seen. Strong increases in the temperature are evident both in reconnecting current layers and within magnetic islands. In the current layers T_{\perp} typically exceeds T_{\parallel} . Within magnetic islands T_{\parallel} is largest and forms distinct high temperature rings. One source of the hot ions within islands is the ejecta of heated ions from the current layers. However, the hot rings within islands appear disconnected from current layers. The enhancement of T_{\parallel} compared with T_{\perp} suggests that the ion contraction mechanism that was proposed earlier as a mechanism for heating electrons (Drake et al. 2006) is also active for ions. This mechanism requires that particles bounce several times within an island during its contraction and therefore that the particle velocity be super-Alfvénic. Evidently this is easier for electrons than for ions. It is evident from Fig. 3 that the fraction of super-Alfvénic ions is significant and the results from Fig. 4 are consistent with the contraction mechanism.

Anomalous cosmic rays are accelerated from LISM neutral particles that are ionized deep in the heliosphere, picked-up by the supersonic solar wind and carried out to the TS and heliosheath. The temperature of these ions is around $1keV$ upstream of the TS and the pickup ions are probably heated to $10keV$ at the TS although neither Voyager is able to directly measure all of these high temperature ions (Decker et al. 2008; Richardson et al. 2008). The background ions have a temperature of around $10eV$ downstream of the shock. As discussed previously, to explore how high temperature ions are accelerated during reconnection, we carried out simulations with 5% of the ions having an initial temperature 30

times that of the background. This fractional number density is less than the realistic value of around 30%. The actual pickup temperature is closer to 1000 times that of the background but the value used in the simulation is an upper limit based on the requirement that these particles remain magnetized in our limited computational domain. In Fig. 3(c) we show the initial and final ($\Omega_p t = 200$) ion energy spectra. The energy distribution at late time maintains an exponential form. In Fig. 5(a) the locations of all ions with energies above $188m_i c_A^2$ at $\Omega_p t = 150$ are shown superimposed on a background of the electron current J_{ez} . The most energetic ions are clustered around three locations: $x, y = 160d_p, 180d_p$; $x, y = 60d_p, 210d_p$; and $x, y = 140d_p, 360d_p$. Each of these locations is within a large island where two islands had at an earlier time merged. The merging process at these sites is evident in the the out-of-plane current J_{ez} in Fig. 2(b) and the ion temperature data in Fig. 4 at $\Omega_p t = 136$, which is the time at which the rate of energy gain of the ACR seed particles maximizes.

Detailed studies of the orbits and energy gain of test protons have been carried out using the electric and magnetic fields from the simulation at $\Omega_p t = 136$, corresponding to Fig. 2(b). The particles were initialized with thermal distributions corresponding to $T_p = 12.5m_p c_A^2$, the energy of the seed ACRs, and randomly distributed in the vicinity of merging islands. In Fig. 5(b) we show two sample trajectories, corresponding to particles which gained the most energy around their respective merging sites. More details of the merging sites can be seen in Fig. 2(b), where the orbits do not obscure the structure of the current layer separating the merging islands. The particles with the greatest energy gain bounce repetitively between the contracting ends of the islands and gain energy during each reflection. The energy gain of the particle orbiting around $y \sim 210d_p$ in Fig. 5(b) is shown versus horizontal position y in Fig. 5(c). The sharp increase in the energy during each reflection is evident. The energy gain of this proton exhibits the classic signatures of a first order Fermi process. Thus, we conclude that the merging of two islands causes a contraction of the resulting larger-scale island, which boosts the energy of ions circulating within the larger island. Thus, the island contraction mechanism seems to be responsible for the energy gain of the most energetic ions in the simulation. Ions also gain energy within the outflow jets of each of the current layers, as shown in Fig. 4 and as discussed earlier (Drake et al. 2009).

The basic physics of particle acceleration in contracting islands, which was seen in early test particle simulations (Kliem 1994), was first discussed in detail in the context of electron acceleration (Drake et al. 2006). In Appendix A the basic concepts are reviewed. As islands contract, particles that circulate around islands sufficiently fast conserve their parallel (to \mathbf{B}) action $v_{\parallel}L$, with v_{\parallel} the parallel velocity and L the length of the field line. Island contraction shortens L and therefore increases v_{\parallel} . However, the corresponding reduction of the magnetic field B during contraction causes the perpendicular velocity v_{\perp} to decrease (due to the conservation of the magnetic moment). During infinitesimal contractions in an isotropic

plasma the two effects cancel and there is no net energy gain. This result is consistent with Parker’s transport equation (Parker 1965), which was derived in the limit of strong scattering, where the energy gain is linked to plasma compression. Since 2-D island contraction preserves the area within the island (Fermo et al. 2009) and is therefore nearly incompressible, the Parker equation has no energy gain term corresponding to island contraction. However, as shown in Appendix A when an island undergoes a finite contraction, the parallel energy gain dominates and as a result the rapidly circulating particles gain net energy. This result, of course, requires that there is no mechanism for scattering particles that is sufficiently strong to maintain the isotropy of the plasma pressure as island contraction takes place.

The spatial differences between the parallel and perpendicular temperatures in Fig. 4 are evidence that if some mechanism does cause particle scattering in the simulations, it is sufficiently weak to allow significant pressure anisotropies to develop during island growth and merger. To put this on a more quantitative basis, in Fig. 6 we show data showing the distribution of $\beta_{\parallel} = 8\pi p_{\parallel}/B^2$ and $\beta_{\perp} = 8\pi p_{\perp}/B^2$ at three times from the simulation of Fig. 3(a,b) (no ACR seed particles). Each point is from a single grid point of the simulation. The two curves are the marginal stability boundaries for the firehose,

$$\beta_{\parallel} = \beta_{\perp} + 2, \tag{2}$$

and mirror instabilities,

$$\beta_{\parallel} = \frac{\beta_{\perp}^2}{1 + \beta_{\perp}}. \tag{3}$$

Points below the lower curves are in the region of firehose instability while those above the upper curves are in the region of mirror mode instability. Both instabilities act to isotropize the plasma in their respective regions of instability. We emphasize, of course, that these stability boundaries are based on simple homogeneous models and do not reflect the complex geometry of reconnecting islands. At early time in Fig. 6(a) the bulk of the plasma is nearly isotropic with a few scattered points lying in the mirror unstable region. At $\Omega_p t = 84$ in Fig. 6(b), which is a time of strong reconnection and particle energy gain in this simulation, significant anisotropy has developed and the data has spilled into the unstable regions of both the mirror and firehose instabilities. At late time in Fig. 6(c) the plasma has largely retreated into the stable region between the two stability boundaries. The firehose condition in particular appears to significantly constrain the increase in β_{\parallel} . Although plotted in a slightly different format, the data in Fig. 6(c) bears a striking similarity to data from the slow solar wind (Hellinger et al. 2006; Bale et al. 2009). In the data from the solar wind, as in the present simulation, the plasma bumps up against the theoretical stability boundaries of the mirror and oblique firehose stability boundaries. Moreover, in the solar wind enhanced magnetic fluctuations are measured close to the stability boundaries, suggesting that the two

instabilities are limiting the plasma anisotropy (Bale et al. 2009). The overall increase in the number of points at higher values of β_{\parallel} and β_{\perp} with increasing time in Fig. 6 reflects the strong plasma heating and the reduction in the magnetic energy as the simulation develops. This data demonstrates that, while the plasma dynamics act to limit the level of anisotropy, significant anisotropies do develop, which, as shown in the Appendix, is a requirement for net energy gain to take place during island contraction.

It has been suggested previously that the increase in parallel electron energy through island contraction would be limited by the firehose instability (Drake et al. 2006). In an anisotropic plasma the tension force \mathbf{F}_t of bent magnetic field fields takes the form,

$$\mathbf{F}_t = \left(1 - \frac{\beta_{\parallel} - \beta_{\perp}}{2}\right)\mathbf{B} \cdot \nabla\mathbf{B}. \quad (4)$$

As the firehose marginal condition is approached the tension force goes to zero and island contraction stops, halting reconnection and the associated acceleration of particles. In the Appendix this behavior is shown in a simple model of a contracting flux loop. In Fig. 7 we present data from $\Omega_p t = 200$, corresponding to Fig. 6(c), on the spatial distribution of regions where the firehose and mirror stability boundaries are violated. In Fig. 7(a) is the out-of-plane current, which shows that structure of islands at this time. In Fig. 7(b,c) the black marks the regions where the firehose and mirror conditions are violated, respectively. As expected from Fig. 4, the islands are regions where the firehose condition is violated while the x-line regions and separatrices are where the mirror condition is violated. The firehose condition in Fig. 7(b) combined with the results of Fig. 6(c) strongly suggest that in our simulations the firehose condition does play a central role limiting island contraction during reconnection, consistent with the model presented in the Appendix.

Further evidence that the island contraction mechanism plays the dominant role in heating the highest energy particles can be gleaned from the energy spectra in Fig. 3(c). A model equation for the the omnidirection particle distribution function $F(v, t) = 4\pi v^2 f(v, t)$ in a homogeneous system is given by

$$\frac{\partial F}{\partial t} + \frac{\partial}{\partial v} \dot{v} F = -\frac{F}{\tau}, \quad (5)$$

where \dot{v} is the rate of increase in the particle speed and τ is the loss rate of particles from the acceleration region. For the simulations there is no particle loss so $\tau \rightarrow \infty$ and the change in F during a short time interval δt is given by

$$\delta F \simeq -\delta t \frac{\partial}{\partial v} \dot{v} F \simeq \frac{\dot{E} \delta t}{T_i} F, \quad (6)$$

where $E = mv^2/2$ is the energy, we have taken F to be a Maxwellian with a temperature T_i

and for $E \gg T_i$ the velocity derivative acts only on F . Thus,

$$\delta(\ln F) \simeq \frac{\dot{E}\delta t}{T_i}. \quad (7)$$

Consistency with Fig. 3(c), in which the increment of $\ln F$, increases linearly with E , requires that $\dot{E} \propto E$, which suggests that the energy gain is through a first order Fermi process.

In the island contraction mechanism the average rate of energy gain is proportional to $\langle c_A/L \rangle$, where c_A is the Alfvén speed based on the magnetic field of the island before contraction and L is the associated island length. The brackets denote an average over the islands in the system. We estimate this average for the simulation of Fig. 4(c) at $\Omega_p t = 136$ by computing the average of $|(\mathbf{B} \cdot \nabla \mathbf{B})/B|$. The result is $0.05B_0/d_p$, which corresponds to $L \sim 20d_p$. This scale is consistent with the size of the islands in Fig. 4. From the rate of change of $\ln F$ during the time interval $\Omega_p t = 100 - 150$ we calculate the rate of ion energy gain,

$$\dot{E} = 0.05 \langle \frac{c_A}{L} \rangle E. \quad (8)$$

The factor 0.05 represents the weighted area where islands are undergoing contraction.

4. ACR spectra resulting from reconnection

The reconnection of the sectorized magnetic field dissipates most of the magnetic free energy. The simulations presented in Sec. 3 demonstrated that reconnection of the sectorized field accelerates seed ACRs through the magnetic island contraction mechanism, which is a first order Fermi process. Furthermore island contraction is regulated by the approach to the firehose marginal stability condition (Figs. 6 and 7). However, the PIC simulations can not produce the expected ACR energy spectrum because the islands are unrealistically small, and therefore do not have enough flux to contain $100MeV/\text{nucleon}$ ions, and because a loss mechanism is needed to balance the source in the energy drive equation to obtain a steady state spectrum.

Knowing the functional form of the rate of energy gain of energetic ions from the simulations, however, we propose a simple 1-D model equation for the ACR energy spectrum that parallels the 2-D model proposed earlier for electrons (Drake et al. 2006). The basic idea is that the ions that gain significant energy undergo acceleration in a series of contracting islands. As discussed earlier, the energy gain of an ion undergoing Fermi acceleration in a single island is controlled by the invariance of the parallel action. The action invariant limits the ion energy gain in a single contraction and requires particles undergoing significant energy gain to interact with many islands (Drake et al. 2006). What was also shown

earlier (Drake et al. 2006) was that particles undergoing acceleration slowly drift outwards in the island and eventually cross a narrow boundary layer at the separatrix bounding the island. During the crossing of the boundary layer, which has a scale length controlled by electrons, the pitch angle of the particles is scattered. Because the Larmor radius of ions is greater than that of electrons, the ions are even more effectively scattered – the trajectories of the most energetic particles in Fig. 5 are only marginally magnetized. Thus, the particles will undergo acceleration in a series of contracting islands, starting with an approximately isotropic distribution at the beginning of each contraction. This perhaps understates the rate of ion acceleration since it is possible that p_{\parallel} may be greater than p_{\perp} as contraction initiates. The rate of gain of energy of ions of a given energy can be calculated by averaging over the rate of energy gain over the distribution of islands in the simulation as shown in Eq. (1). If particle acceleration begins in a system in which the plasma β is initially very low, we show in the Appendix that, as expected, the contraction velocity u of the island is the Alfvén speed. As time passes the energetic particle pressure builds up. When the initial normalized particle pressure β approaches unity, the island can only contract a small amount until the marginal firehose condition is reached and the tension force that drives reconnection goes to zero, contraction stops and particle energy gain ceases. This was demonstrated explicitly in the case of electrons (Drake et al. 2006). The violation of the marginal firehose condition within islands in Fig. 7 demonstrates that the same important feedback on the islands is taking place at the ion scales. That feedback is a critical element of any reconnection driven particle acceleration model was an important conclusion of an MHD study of reconnection that included the dynamics of test particles (Onofri et al. 2006).

To model the shutoff of particle acceleration as the plasma β rises (see Eq. (A9)), we take a simple form for the contraction velocity,

$$u = c_A \left(1 - \frac{4\pi p}{B^2} \right)^{1/2} \quad (9)$$

with p the ACR pressure. Averaging over the distribution of islands in the simulation we obtain the averaged rate of ion energy gain

$$\frac{dE}{dt} = 0.05 \left\langle \frac{c_A}{L} \right\rangle \left(1 - \frac{4\pi p}{B^2} \right)^{1/2} E, \quad (10)$$

which differs from the result benchmarked with the simulation data in Eq. (8) only by the factor within the parenthesis reflecting inability of islands to contract as β approaches unity. To facilitate a direct evaluation of the energy spectra, we consider a simple 1-D model for the omnidirectional distribution function $F(v, t)$ in which convective loss is simply represented as a loss time τ_L . Using the result in Eq. (10) to calculate the rate of convection \dot{v} in phase

space, we obtain the equation for F ,

$$\frac{\partial F}{\partial t} + \frac{1}{\tau_h} \left(1 - \frac{4\pi p}{B^2}\right)^{1/2} \frac{\partial}{\partial v} vF = -\frac{1}{\tau_L} (F - F_0); \quad (11)$$

where the ACR pressure is given by

$$p = \int_0^\infty dv F(v, t) m v^2, \quad (12)$$

$1/\tau_h = 0.025 \langle c_A/L \rangle$ is the pickup ion heating rate and F_0 is the ACR seed. This equation differs from that presented in Drake et al. (2006) because of the absence of magnetic shear in the sectored heliospheric magnetic field and the 1-D assumption.

The particle loss represented by τ_L limits the energy gain of the ACRs. Since the ions are trapped by the magnetic islands, the loss rate is controlled by the large-scale convective flows in the HS shown in Fig. 1. Thus, τ_L is energy independent and is of the order of the heliospheric convection time, which can become very long near the stagnation point of the flow near the HP. The heating time is the Alfvén transit time across a sector and, in contrast with the loss time, decreases near the heliopause due to the increase of c_A and the reduction of the sector spacing (see Fig. 1). We therefore conclude that $\tau_L \gg \tau_h$ in the sectored region of interest for ACR acceleration.

Equation (11) is an equidimensional equation for sufficiently high velocity where the source F_0 can be neglected. The equation therefore has no intrinsic velocity scale and the solutions in this region are therefore power laws. Fortunately, the steady state solution to Eq. (11) can be written in closed form,

$$F(v) = (\gamma - 1) v^{-\gamma} \int_0^\infty ds s^{\gamma-1} F_0(s), \quad (13)$$

where the power law γ satisfies the equation,

$$(\gamma - 1) \left(1 - \frac{4\pi p_0}{B^2} \frac{\gamma - 1}{\gamma - 3}\right)^{1/2} = \frac{\tau_h}{\tau_L}, \quad (14)$$

and the ACR pressure was evaluated exactly $p = p_0(\gamma - 1)/(\gamma - 3)$ with p_0 the initial pickup particle pressure. The convergence of the ACR pressure requires $\gamma > 3$. We also emphasize that the expression for γ in Eq. (14) is valid only if the seed ACR β is small, which is not generally valid within the heliosheath but as shown in Fig. 1(b) is valid close to the heliopause. It is only in this low β region that the magnetic field has sufficient energy to raise the pickup seed particles to energies typical of the ACRs. Equation (14) has simple solutions in the limit of large and small τ_h/τ_L as follows:

$$\gamma = \frac{\tau_h}{\tau_L} \quad \tau_h/\tau_L \gg 1 \quad (15)$$

$$\gamma = 3 + \beta_0 \quad \tau_h/\tau_L \ll 1, \quad (16)$$

where $\beta_0 = 8\pi p_0/B^2$ is the initial pickup β .

5. DISCUSSION AND IMPLICATIONS

The energy spectra of the ACRs have continued to unroll as the Voyager spacecraft have moved further into the HS and there is evidence that the source region of the higher energy particles has now been reached (Stone et al. 2008). The spectral indices of the ACR H and He spectra are around 1.75. In the reconnection model presented here the power law index of the differential energy spectrum is $\gamma/2 = (3 + \beta_0)/2$. The MHD data shown in Fig. 1(b) indicate that close to the HP the plasma β drops to 0.5 so the estimated spectral index of the reconnection model approaches 1.75, which is close to the value observed.

A central question, of course, is whether the rate of energy gain due to reconnection is sufficient to produce ACRs in the range of $100\text{MeV}/\text{nuc}$. The heating rate in Eq. (8) depends on the typical Alfvén transit time across a magnetic island. The characteristic scale length of the magnetic islands is the sector spacing. An upper limit on the sector spacing is given by the 13 day sector periodicity times the local heliosheath velocity, which is around $100\text{km}/\text{s}$ (Richardson et al. 2008). Based on a local magnetic field of 0.15nT (Burlaga et al. 2006) and a density of $0.002/\text{cm}^3$ (Richardson et al. 2008), we obtain an Alfvén velocity of $74\text{km}/\text{s}$. The Alfvén transit time across a typical magnetic island is therefore 18 days. From Eq. (8) the characteristic heating time τ_h is around a year. The compression of the magnetic field and reduction of the density near the HP can increase c_A by a factor of three, which reduces the heating time to 120 days. The total e-folding time to increase the $10\text{keV}/\text{nuc}$ pickup ions to $100\text{MeV}/\text{nuc}$ therefore ranges from 3 to 9 years. The convective flow out of the sector field in the latitudinal direction very likely dominates the loss of energetic particles. For a sector-zone spanning 30° the characteristic width of the sector zone at a HP distance of 150AU is around 75AU . A transverse velocity of $30\text{km}/\text{s}$ or $6\text{AU}/\text{year}$ yields $\tau_L = 13$ years, which exceeds τ_h as expected.

A key observation of ACRs is the similarity in the spectra of different species when expressed on a per nucleon basis. In the case of the shock acceleration model this result is because the rate of energy gain of a particle as it reflects back and forth across the shock is on average independent of mass when expressed on a per nucleon basis (Blandford & Eichler 1987). The contracting island mechanism for particle energy gain is analagous – upon reflection from the end of a contracting island, the rate of energy gain is independent of mass when expressed on a per nucleon basis. In particular, the particle distribution functions of the various minor species are also given by the result in Eq. (13), where F_0 is the distribution

of seed particles of a given species but the spectral index γ is controlled by H with some contribution from He. Thus, at high energy the spectra of all of the minor species take the form of power laws with the same spectral indices as H.

A surprising observation is the nearly universal $f \propto v^{-5}$ spectrum of super-Alfvénic ions observed in the quiet-time solar wind throughout the heliosphere (Fisk & Gloeckler 2006). These distributions correspond to $F \propto v^{-3}$ or $F \propto E^{-1.5}$, the low β limit of Eq. (14). An explanation of this universal spectral index has been offered based on ion acceleration in compressible turbulence (Fisk & Gloeckler 2006). We suggest that the non-pickup ions accelerated through reconnection within the heliosheath could be the source of this near universal spectrum of super-Alfvénic particles. Since the pressure of the non-pickup particles is much less than that of the pickup particles, they can be treated as minor species just like the minor ACRs. Since they start from lower energy they never reach energies associated with ACRs, but like the minor species their spectral index is controlled by that of the pickup protons. In the limit of low β_0 , of course, the spectral index is 1.5. The spectral index of 1.5 arises from the approach to the marginal firehose condition of the ACR protons. An important question is whether such a spectrum of super-Alfvénic ions can move upstream across the TS and into the inner heliosphere. An exploration of the transport of such particles is beyond the scope of the present manuscript but should be pursued.

Finally, we note that the reconnection of the sectored magnetic field in the heliosheath was independently proposed as the source of the ACRs by Lazarian & Opher (2009), denoted by LO in the following. Beyond the basic idea that the sectored field is a source for ACR acceleration and that the compression of the sectors on the approach to the heliopause would enhance the likelihood that reconnection would take place, the LO model is very different from that discussed here. Reconnection in the LO model is based on the turbulent reconnection model of Lazarian & Vishniac (1999) although the explicit source of the turbulence is not identified. In the model presented in this manuscript reconnection is collisionless and fast reconnection is facilitated by the Hall term in Ohm’s law (Birn et al. 2001). Recent scaling studies (Shay et al. 2007) and observations (Phan et al. 2007) confirm that Hall reconnection remains fast even in systems comparable in size to that defined by the sector spacing close to the HP. Further, in the model presented here the interaction of islands on adjacent current layers facilitates the rapid dissipation of the magnetic energy in the sectored region. While the mechanism for particle acceleration in both models is a first order Fermi process, the LO model is based on periodic reflection from the plasma flowing inward toward the x-line (Lazarian 2005) and curiously is taken in the strongly relativistic limit and so does not apply to ACRs. There is no evidence in even the largest scale PIC simulations carried out to date that such a mechanism is active during reconnection (see the particle distributions in Fig. 2 of Drake et al. (2009)). On the other hand it can’t be ruled out that some additional source

of turbulence and associated scattering could alter the particle dynamics allowing particle acceleration as proposed by Lazarian (2005) to take place. One might make the case that the particles moving along the trajectories shown in Fig. 5 are reflecting from the inflow of the reconnecting islands and the acceleration mechanism is therefore similar to that of the LO model. However, the spectra resulting from this acceleration process are not given by the Lazarian (2005) model.

This work has been supported by NSF Grant PHY-0316197 and NASA Grant NNG06GH23G. M. O. acknowledges the support of a NASA-Voyager Guest Investigator grant NNX07AH20G and an NSF CAREER Grant ATM-0747654. Computations were carried out at the National Energy Research Scientific Computing Center and the NASA Ames Research Center.

A. Particle acceleration during island contraction

The magnetic energy that is released during magnetic reconnection takes place as bent magnetic fields downstream from the x-line straighten out, driving the outflow exhaust. In the Petschek model the bent fields take the form of slow shocks that both drive the outflow and heat the plasma. During reconnection in a multi-island environment, the contraction of magnetic islands releases magnetic energy – initially oblate islands try to become round (Drake et al. 2006). The merging and contraction of islands is a nearly incompressible process (Fermo et al. 2009). In magnetic reconnection, therefore, particle acceleration is through incompressible flows in contrast with shocks, where particle energy gain as described by Parker’s equation is explicitly driven by plasma compression.

A fundamental question is therefore whether the incompressible flows which dominate the dynamics of islands during reconnection can accelerate particles through a first-order Fermi process or it is necessary to identify another mechanism for particle acceleration. If a first order Fermi mechanism does take place in the presence of incompressible flows, how do we resolve the apparent contradiction with the Parker equation and the conventional wisdom that first-order Fermi acceleration requires compressible plasma motion?

To make analytic progress, we consider a simple 2-D elongated ring of magnetic flux in the shape of a racetrack with an initial length along a field line L_0 and an initial width (of the track) w_0 such that $L_0 \gg w_0$. The magnetic field in the flux tube is taken to be B_0 . The flux tube is not in equilibrium, which is not an issue because we are interested in test particle behavior as the ring contracts. During contraction, the flux $\psi_0 = Bw$ is conserved as is the total area $A_0 = Lw$ of the flux tube so the magnetic field B can be calculated as a function of its initial value as $B = B_0L/L_0$. The constants of the particle motion are the

magnetic moment $\mu = mv_{\perp}^2/B$ and the longitudinal action $J_{\parallel} = v_{\parallel}L$. These invariants allow us to calculate the particle velocity v in terms of the initial velocities and L ,

$$v^2 = v_{\perp 0}^2 \frac{L}{L_0} + v_{\parallel 0}^2 \frac{L_0^2}{L^2}. \quad (\text{A1})$$

If we linearize this result by assuming that L changes by only a small amount ΔL , we find the change in v^2 ,

$$\Delta v^2 = (v_{\perp 0}^2 - 2v_{\parallel 0}^2) \frac{\Delta L}{L_0}. \quad (\text{A2})$$

This result is equivalent to that obtained by (Cho & Lazarian 2006) in their evaluation of particle acceleration in incompressible MHD turbulence if their parallel flow velocity is equated with the rate of change of the field line length. For an initially isotropic plasma $v_{\perp 0}^2 = 2v_{\parallel 0}^2$ (in an averaged sense) so the energy gain is zero. This is because the increase in the parallel energy (conservation of J_{\parallel}) is balanced by a reduction of the perpendicular energy (conservation of μ and the decrease in B). This result is consistent with the Parker equation, in which there is no energy gain for incompressible flows since the Parker equation was derived under the assumption of strong scattering. On the other hand, even if the plasma is initially isotropic a large contraction or stretching of the island increases the particle energy,

$$v^2 = v_0^2 \left(\frac{2L}{3L_0} + \frac{L_0^2}{3L^2} \right), \quad (\text{A3})$$

assuming that there is no scattering during contraction. Stretching is magnetically unfavorable and is therefore of less interest during reconnection and island merger. The result in Eq. (A3) is consistent with the PIC simulations of island contraction (Drake et al. 2006), which started with an initial elongated island in a nearly isotropic plasma but nevertheless revealed strong parallel heating of electrons and substantial net energy gain. To the extent that nearly collisionless plasma can maintain anisotropy, with limits perhaps controlled by the firehose or a related marginal stability condition, contracting islands drive particle acceleration through a first-order Fermi process.

To gain further insight into how the full distribution of particles gains energy during the contraction of an island and the role of the firehose condition, we consider an elongated island of length L_0 with an initially isotropic distribution of particles with initial pressure p_0 . The parallel and perpendicular pressures during contraction are given by

$$p_{\parallel} = p_0 \frac{L_0^2}{L^2}, \quad p_{\perp} = p_0 \frac{L}{L_0}. \quad (\text{A4})$$

Writing an energy equation for the contracting loop, including the internal energy $(p_{\parallel} + 2p_{\perp})/2$, the magnetic energy $B^2/8\pi$ and the flow energy associated with the contraction

velocity u , $\rho u^2/2$, we find

$$\frac{u^2}{c_{A0}^2} + \left(\frac{L^2}{L_0^2} - 1 \right) + \frac{\beta_0}{2} \left(\frac{L_0^2}{L^2} + 2\frac{L}{L_0} - 3 \right) = 0, \quad (\text{A5})$$

where $c_{A0}^2 = B_0^2/4\pi\rho$ and $\beta_0 = 8\pi p_0/B_0^2$. In Eq. (A5) the first term is the flow energy, the second the change in magnetic energy and the third the change in internal energy. In writing this equation we have ignored geometrical factors of order unity that enter the flow energy due to the fact that the convective velocity varies over the length of the island. In the absence of the pressure (the limit of low β_0), the reduction of the magnetic energy as L decreases well below L_0 causes u to increase up to the Alfvén speed. However, if β_0 is not too small, the increase in the total internal energy can balance the reduction in magnetic energy so that u takes on a maximum value. Taking the differential of the second two terms with respect to L yields an equation for the value of L at the peak velocity;

$$2\frac{L}{L_0} + \beta_0 \left(1 - \frac{L_0^3}{L^3} \right) = 0. \quad (\text{A6})$$

This condition is precisely the marginal firehose condition

$$p_{\parallel} - p_{\perp} - \frac{B^2}{4\pi} = 0. \quad (\text{A7})$$

Thus, the rate of island contraction continues to increase with p_{\parallel} increasing compared with p_{\perp} until the marginal firehose condition is violated at which point the net force driving loop contraction drops to zero. Since loop contraction is the driver of reconnection, this causes reconnection to cease.

It is illuminating to compare the maximum contraction velocity u in the low and high β_0 limits. At low β_0 the maximum velocity occurs for $L/L_0 = (\beta_0/2)^{1/4}$ and

$$u \simeq c_{A0}, \quad \beta_0 \ll 1, \quad (\text{A8})$$

while for β_0 large $L/L_0 \simeq 1 - 2/(3\beta_0)$ and

$$u \simeq \frac{2c_{A0}}{\sqrt{3\beta_0}}, \quad \beta_0 \gg 1. \quad (\text{A9})$$

Thus, at high β_0 only a very small contraction of the island takes place and the contraction velocity and associated particle acceleration are weak.

REFERENCES

Alexashov, D., & Izmodenov, V. 2005, *Astron. & Astrophys.*, 439, 1171

- Bale, S. D., Kasper, J. C., Howes, G. G., Quataert, E., Salem, C., & Sundkvist, D. 2009, submitted
- Birn, J., et al. 2001, *J. Geophys. Res.*, 106, 3715
- Blandford, R. D., & Eichler, D. 1987, *Physics Reports*, 154, 1
- Burlaga, L. F., Ness, N. F., & Acuna, M. H. 2006, *ApJ*, 642, 584
- Burlaga, L. F., Ness, N. F., Acuna, M. H., Lepping, R. P., Connerney, J. E. P., & Richardson, J. D. 2008, *Nature*, 454, 75
- Burlaga, L. F., Ness, N. F., Acuna, M. H., Lepping, R. P., Connerney, J. E. P., Stone, E. C., & McDonald, F. B. 2005, *Science*, 309, 2027
- Burlaga, L. F., Ness, N. F., & Richardson, J. D. 2003, *J. Geophys. Res.*, 108, 8028
- Cassak, P., Shay, M. A., & Drake, J. F. 2005, *Phys. Rev. Lett.*, 95, 235002
- Cho, J., & Lazarian, A. 2006, *ApJ*, 638, 811
- Crooker, N. U. 1979, *J. Geophys. Res.*, 84, 951
- Cummings, A. C., & Stone, E. C. 1996, *Space Sci. Rev.*, 78, 117
- . 2007, *Space Sci. Rev.*, 130, 389
- Decker, R. B., Krimigis, S. M., Roelof, E. C., Hill, M. E., Armstrong, T. P., Gloeckler, G., Hamilton, D. C., & Lanzerotti, L. J. 2008, *Nature*, 454, 67
- Drake, J. F., et al. 2009, *J. Geophys. Res.*, 114, A05111
- Drake, J. F., Swisdak, M., Schoeffler, K. M., Rogers, B. N., & Kobayashi, S. 2006, *Geophys. Res. Lett.*, 33, L13105
- Egedal, J., Daughton, W., Drake, J. F., Katz, N., & Le, A. 2009, *Phys. Plasmas*, 16, 050701
- Fermo, F. L., Drake, J. F., & Swisdak, M. 2009, ArXiv e-prints
- Fisk, L. A., & Gloeckler, G. 2006, *ApJ*, 640, L79
- Fisk, L. A., Gloeckler, G., & Zurbuchen, T. H. 2006, *ApJ*, 644, 631
- Gosling, J. T., Eriksson, S., Phan, T. D., Larson, D. E., Skoug, R. M., & McComas, D. J. 2007, *Geophysical Res. Lett.*, 34, L06102

- Gosling, J. T., Skoug, R. M., & McComas, D. J. 2005, *Geophys. Res. Lett.*, 110, A01107
- Hellinger, P., Travnicek, P., Kasper, J. C., & Lazarus, L. J. 2006, *Geophys. Res. Lett.*, 33, L09101
- Hesse, M., Kuznetsova, M., & Birn, J. 2001, *J. Geophys. Res.*, 106, 29831
- Huba, J. D., & Rudakov, L. I. 2002, *Phys. Plasmas*, 9, 4435
- Izmodenov, V. V. 2009, *Space Sci. Rev.*, 143, 139
- Kliem, B. 1994, *Ap. J.*, 90, 719
- Lazarian, A. 2005, in *Magnetic fields in the universe*, ed. E. M. de Gouveia Dal Pino, G. Lugones, & A. Lazarian (New York: AIP), 42
- Lazarian, A., & Opher, M. 2009, *ApJ*, 703, 8
- Lazarian, A., & Vishniac, E. 1999, *ApJ*, 517, 700
- Litvinenko, Y. E. 1996, *ApJ*, 462, 997
- Mandt, M. E., Denton, R. E., & Drake, J. F. 1994, *Geophys. Res. Lett.*, 21, 73
- McComas, D. J., & Schwadron, N. A. 2006, *Geophys. Res. Lett.*, 33, L04102
- McNutt, R. L., Lyon, J., & Goodrich, C. C. 1999, *J. Geophys. Res.*, 104, 14803
- Miller, J. A. 1998, *Space Sci. Rev.*, 86, 79
- Miller, J. A., et al. 1997, *J. Geophys. Res.*, 102, 14631
- Onofri, M., Isliker, H., & Vlahos, L. 2006, *Phys. Rev. Lett.*, 96, 151102
- Opher, M., Richardson, J. C., Toth, G., & Gombosi, T. I. 2009, *Space Sci. Rev.*
- Parker, E. N. 1965, *Planet Space Sci.*, 13, 9
- Pesses, M. E., Jokipii, J. R., & Eichler, D. 1981, *Astrophys. J.*, 246, L85
- Phan, T. D., et al. 2007, *Geophys. Res. Lett.*, 34, L14104
- Pritchett, P. L. 2008, *Phys. Plasmas*, 15, 102105
- Pritchett, P. L., Drake, J. F., & Lee, Y. C. 1980, *Phys. Fluids*, 23, 1368

- Richardson, J. D., Kasper, J. C., Wang, C., Belcher, J. W., & Lazarus, A. J. 2008, *Nature*, 454, 63
- Shay, M. A., Drake, J. F., & Swisdak, M. 2007, *Phys. Rev. Lett.*, 99, 155002
- Shay, M. A., Drake, J. F., Swisdak, M., Dorland, W., & Rogers, B. N. 2003, *Geophys. Res. Lett.*, 30, 1345, doi:10.1029/2002GL016267
- Smith, E. J. 2001, *J. Geophys. Res.*, 106, 15819
- Stone, E. C., Cummings, A. C., McDonald, F. B., Heikkila, B. C., Lal, N., & Webber, W. R. 2005, *Science*, 309, 2017
- . 2008, *Nature*, 454, 71
- Tsuneta, S. 1996, *ApJ*, 456, 840
- Wilcox, J. M., & Ness, N. F. 1965, *J. Geophys. Res.*, 70, 5793
- Winterhalter, D., Smith, E. J., Burton, M. E., Murphy, N., & McComas, D. J. 1994, *J. Geophys. Res.*, 99, 6667
- Yamada, M. 2007, *Phys. Plasmas*, 14, 058102
- Zank, G. P., Pauls, H. L., Williams, L. L., & Hall, D. T. 1996, *J. Geophys. Res.*, 101, 21639
- Zeiler, A., Biskamp, D., Drake, J. F., Rogers, B. N., Shay, M. A., & Scholer, M. 2002, *J. Geophys. Res.*, 107, 1230, doi:10.1029/2001JA000287

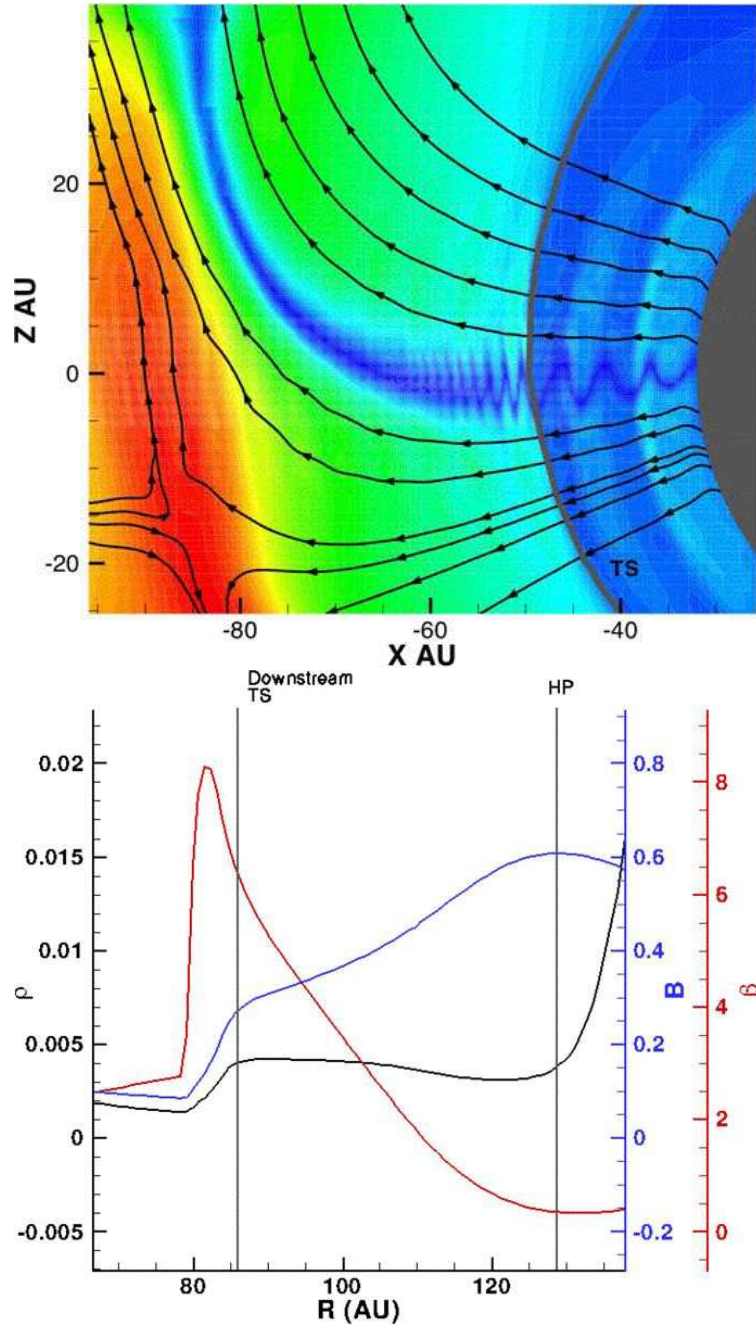


Fig. 1.— (Color online) In (a) the heliospheric magnetic field B and the streamlines of the flow in a cut in the $x - z$ plane from a 3-D MHD simulation with an angle between the rotation axes of the sun and its magnetic field of 7° . The high resolution is this simulation required that the solar wind velocity be reduced to 300km/s to reduce the overall size of the heliosphere. In (b) plots of the magnitude of B in nT , the density ρ in cm^{-3} and β along the stagnation flowline from a simulation without a tilted magnetic field and a solar wind velocity of 417km/s .

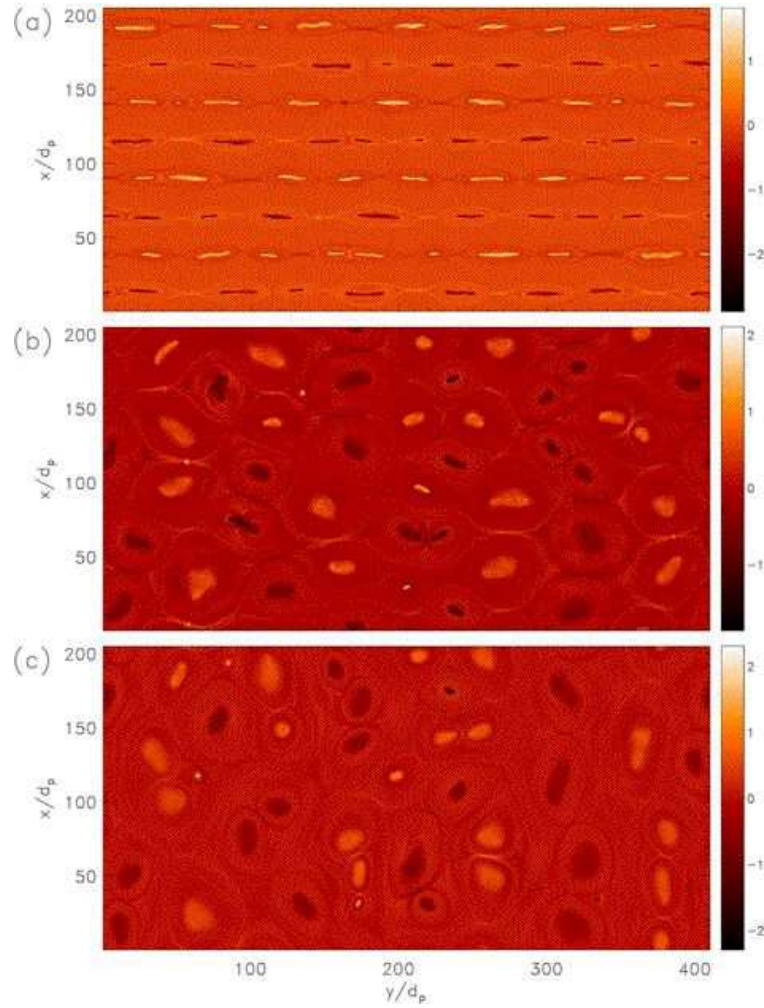


Fig. 2.— (Color online) The out-of-plane current J_{ez} in the $x - y$ plane at three times from a PIC simulation.

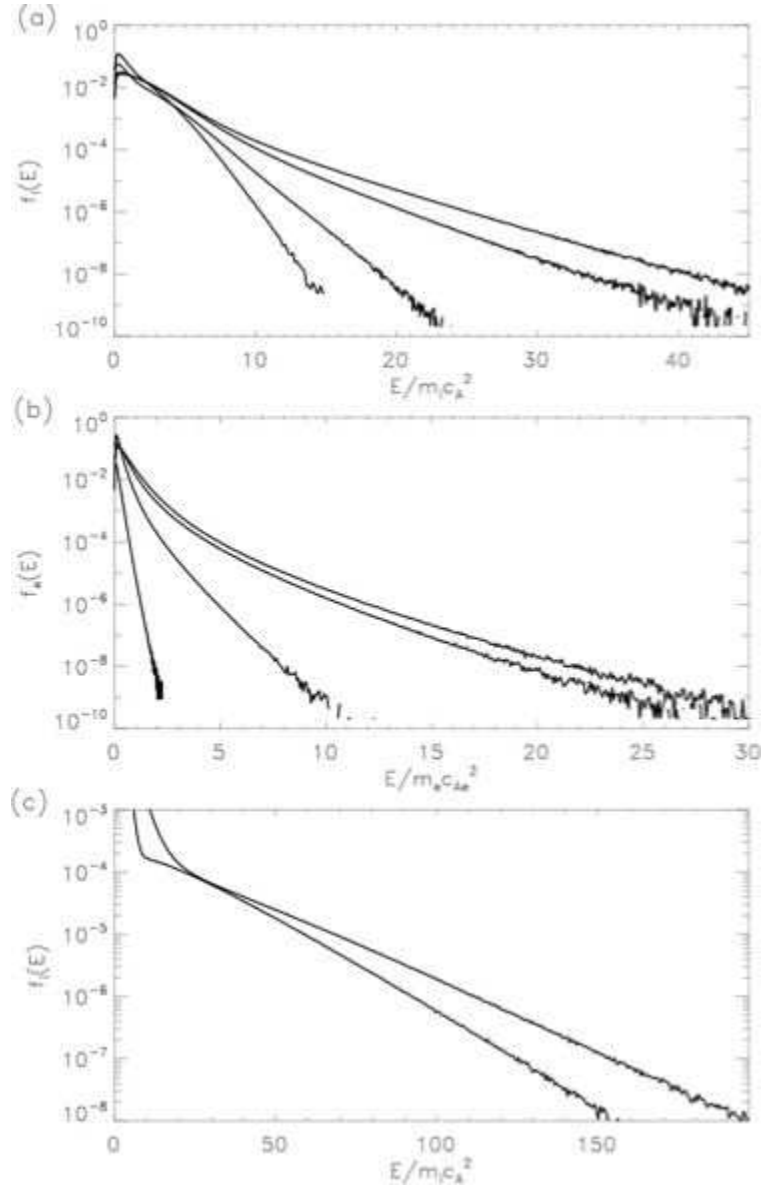


Fig. 3.— The energy spectra of (a) ions and (b) electrons at $\Omega_p t = 0, 50, 100$ and 200 from a PIC simulation without a seed population of pickup ions. In (c) the spectra of ions with a seed population of pickup ions at $\Omega_p t = 0, 200$.

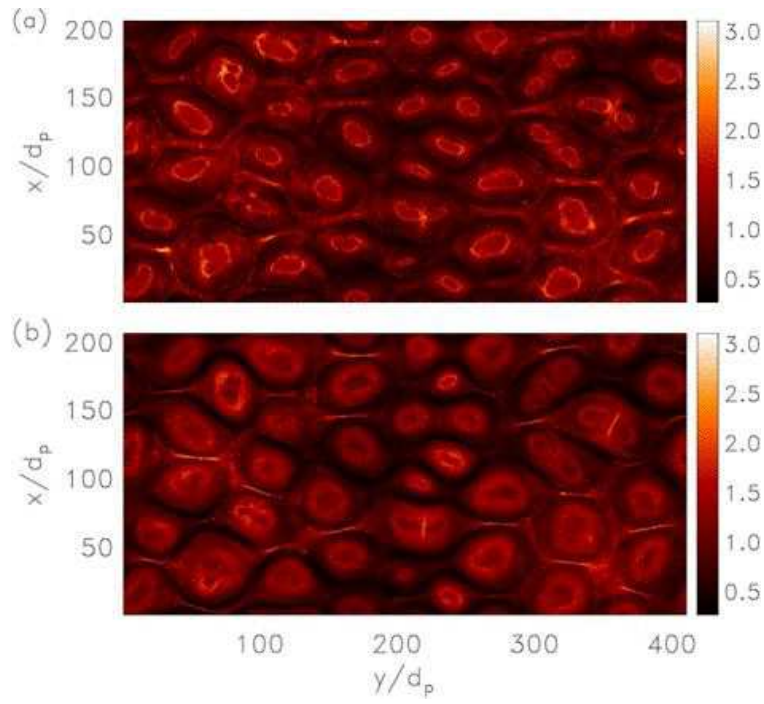


Fig. 4.— (Color online) The ion temperature in the $x - y$ plane (a) parallel and (b) perpendicular to the local magnetic field at $\Omega_p t = 136$ from the simulation in Fig. 2.

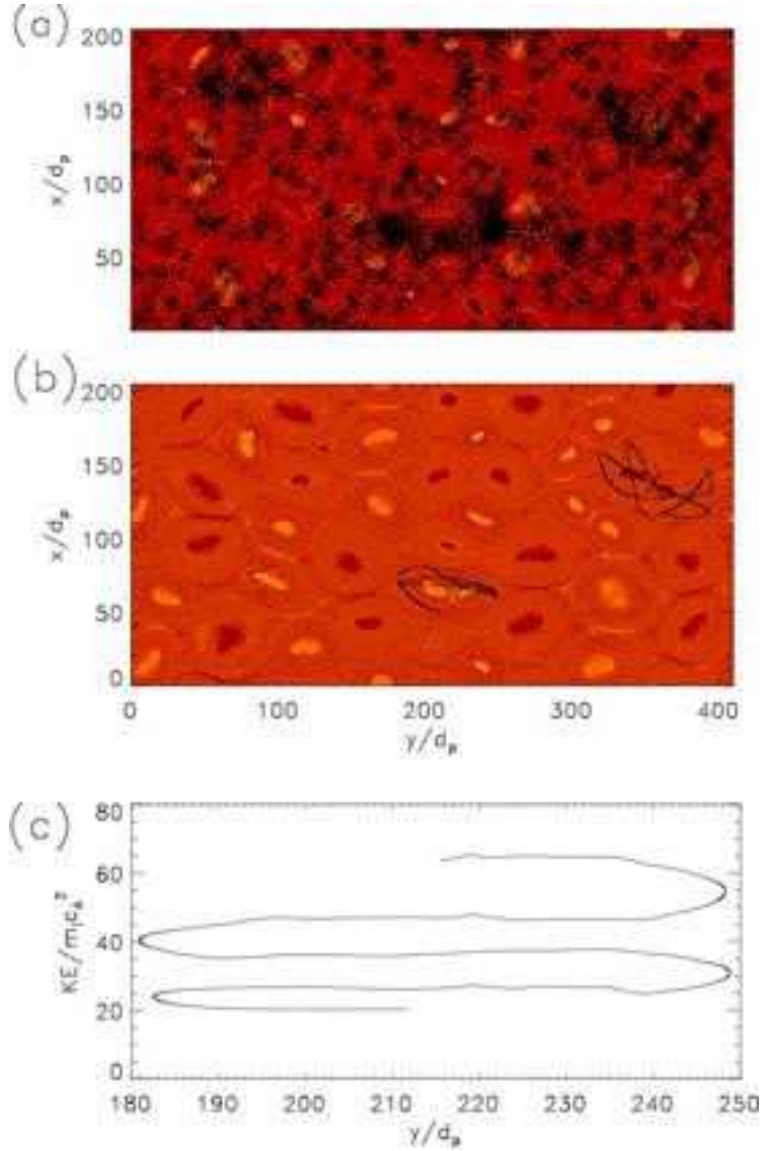


Fig. 5.— (Color online) In (a) the positions of ions with energy exceeding $188m_i c_A^2$ at $\Omega_p t = 150$ in a background of J_{ez} from the simulation in Fig. 2. In (b) the orbits of test protons in the simulation fields at $\Omega_p t = 136$, during the time of most rapid energy gain of the seed ACR particles, plotted over a background of J_{ez} . The particles shown gained the most energy of a group of protons seeded with a thermal spread equal to the ACR seed particles and randomly placed near the two merging sites that contain the most energetic protons in (a). In (c) the energy gain versus horizontal position of the proton orbiting around $y \sim 210d_p$ in (b). The energy gain occurs during reflection from the contracting ends of the island, a first order Fermi process.

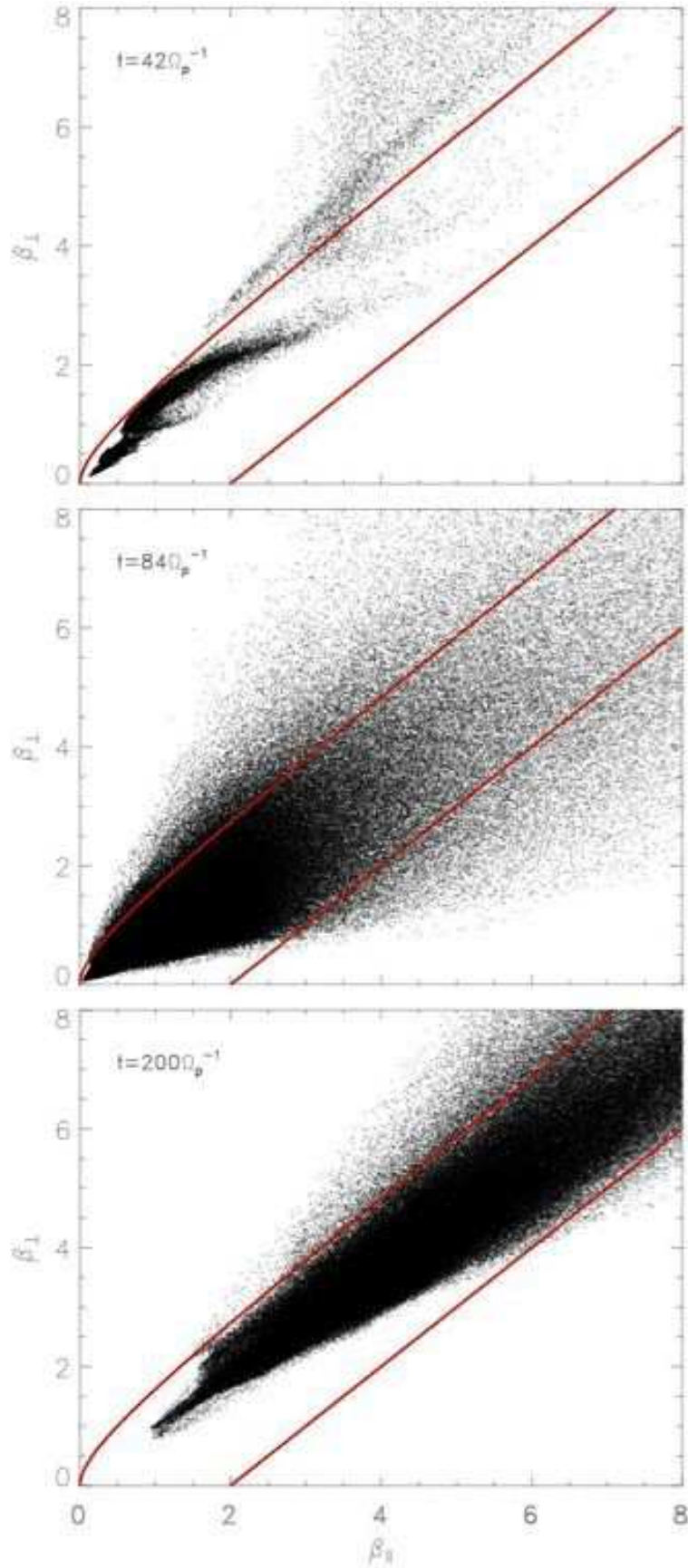


Fig. 6.— (Color online) Shown at three times in the simulation of Fig. 3(c) (no ACR seed

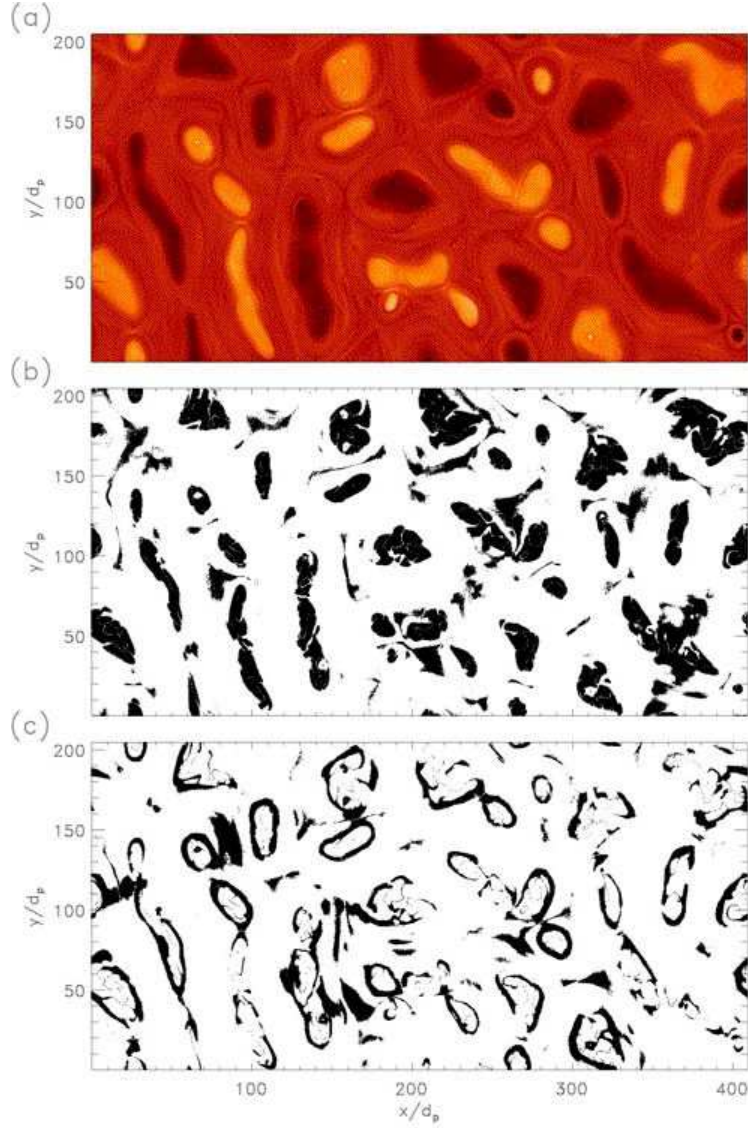


Fig. 7.— (Color online) Data at $\Omega_p t = 200$ from the simulation in Fig. 6. In (a) the out-of-plane current J_z showing the structure of magnetic islands at this time. In (b) and (c) the black denotes regions where the firehose and mirror mode marginal stability conditions are, respectively, violated.